We are IntechOpen, the world's leading publisher of Open Access books Built by scientists, for scientists

4,800
Open access books available

122,000
International authors and editors

135M
Downloads

Our authors are among the

154
Countries delivered to

TOP 1%
most cited scientists

12.2%
Contributors from top 500 universities

CLARIVATE ANALYTICS BOOK CITATION INDEX INDEXED

WEB OF SCIENCE™

Selection of our books indexed in the Book Citation Index in Web of Science™ Core Collection (BKCI)

Interested in publishing with us?
Contact book.department@intechopen.com

Numbers displayed above are based on latest data collected.
For more information visit www.intechopen.com

17

Design of Multi-Passband Bandpass Filters With Low-Temperature Co-Fired Ceramic Technology

Ching-Wen Tang and Huan-Chang Hsu
National Chung Cheng University
Chiayi 621, Taiwan, R.O.C.

1. Introduction

Shared building blocks and power are required for the coexistence of a dual-band multimode wireless local area network and a mobile communication system. Therefore dual-passband bandpass filters have become key components at the front end of a concurrent dual-band receiver. There are several studies on dual-passband filters [1-9]. With sharper passband skirt, lower insertion loss and better selectivity may be resulted in the Zolotarev bandpass filters [1]. In [2], the dual-band filter is constructed with two parallel sets of filters. The frequency-selective resonators [3-6], stepped-impedance resonators [7, 8] and coupled resonator pairs [9] are also employed to design dual-passband filters.
In this article, we use low-temperature co-fired ceramic [10-15] technology to implement the three-dimensional (3D) multi-passband bandpass filters. Figure 1 shows the architecture of the proposed multi-passband bandpass filter, which is composed of multi-sectional short-circuit transmission lines and connected transmission lines. These transmission lines can be transferred individually to multilayered structure. Moreover, the short-circuit transmission lines may make more obvious isolation between passbands [16-18]. As a result, the proposed filter with controllable multiple passbands can be easily achieved by properly choosing the impedance and electrical length of each short-circuit transmission line and the connected transmission line.

2. Equivalent for filter synthesis

The immittance inverter [19] is adopted in this article to analyze the proposed filter. The transformed circuit of a transmission line shown in Fig. 2 can be utilized in the *n*-ordered multi-passband bandpass filter. Moreover, the transformed admittance inverter of the transmission line can be expressed as

$$J_i = Y_i \csc\theta_i \tag{1}$$

where Y_i and θ_i are the corresponding admittance and electrical length of the transmission line, respectively.

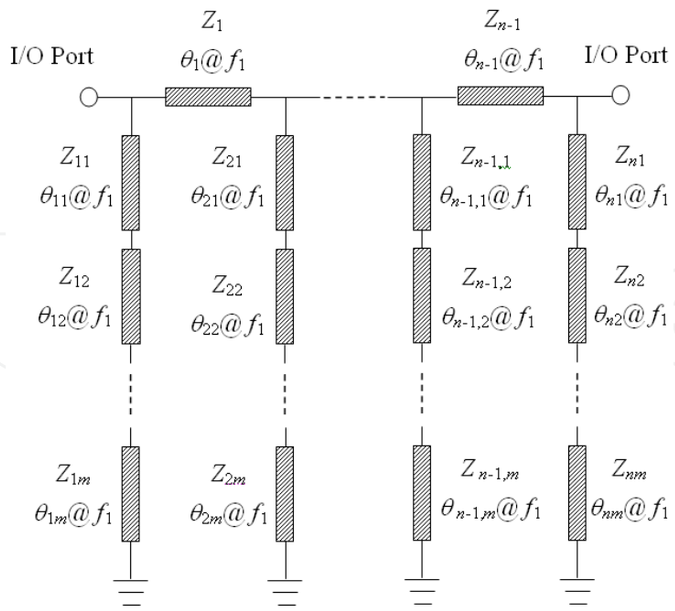

Fig. 1. Architecture of the proposed bandpass filter with multiple controllable passbands

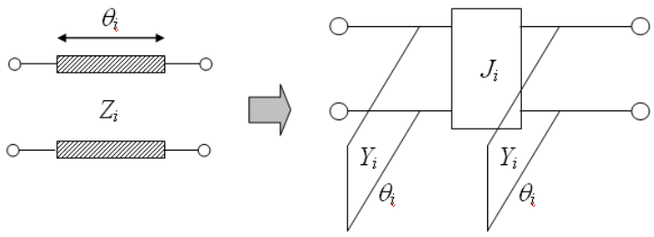

Fig. 2. Transformed circuit of the transmission line

By substituting the transformed transmission lines into the architecture in Fig. 1, the equivalent circuit of the proposed *n*-ordered multi-passband bandpass filter can be obtained as Fig. 3. The susceptance and its slope parameter are, respectively, given by

$$B_i(f) = -\frac{1}{X_{im}(f)} - Y_{i-1}\cot(\frac{f}{f_1}\theta_{i-1}) - Y_i\cot(\frac{f}{f_1}\theta_i), \quad \text{for} \quad i = 1,\cdots,n \tag{2}$$

$$b_i(f_r) = \frac{f_r}{2}\cdot\frac{\partial B_i}{\partial f}\bigg|_{f=f_r}, \quad \text{for} \quad i = 1,\cdots,n \ \text{ and } \ r = 1,\cdots,m \tag{3}$$

where f_r is the central frequency of the *r*th passband with the corresponding fractional bandwidth Δ_r, and

$$X_{ij}(f) = \begin{cases} Z_{im}\tan(\dfrac{f}{f_1}\theta_{im}), & \text{for } j = 1 \\ Z_{i,m-j+1}\cdot\dfrac{X_{i,j-1}(f) + Z_{i,m-j+1}\tan(\dfrac{f}{f_1}\theta_{i,m-j+1})}{Z_{i,m-j+1} - X_{i,j-1}(f)\tan(\dfrac{f}{f_1}\theta_{i,m-j+1})}, & \text{for } j = 2,\cdots,m \end{cases} \tag{4}$$

Moreover, in order to match system's impedance, 50 Ω, the input/output *J*-inerter J_{01} and $J_{n,n+1}$ need to be set as 0.02.

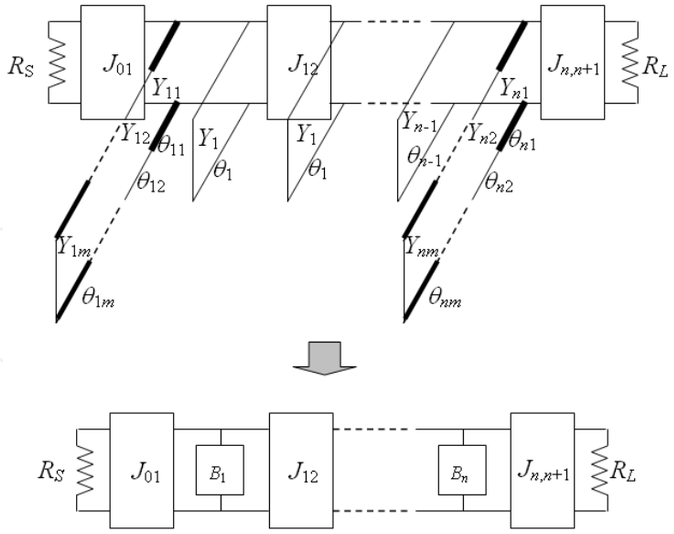

Fig. 3. Equivalent circuit of the proposed *n*-ordered multi-passband filter

As extremely complex procedures are required for generalized formulas to synthesize the proposed multi-passband bandpass filter, only formulas for dual-passband filter synthesis are provided in detail. On the other hand, design examples of the triple- and quadruple-passband filters are offered without detailed equations.

3. Design of the dual-passband filter

To design the dual-passband filters, m = 2 should be selected. Δ_1 and Δ_2 are the corresponding fractional bandwidths of the first and second passband's central frequency, f_1 and f_2, respectively. The susceptances and their slope parameters are, respectively, given by

$$B_i(f) = Y_{i1}\frac{Y_{i1}\tan(\frac{f}{f_1}\theta_{i2})\tan(\frac{f}{f_1}\theta_{i1}) - Y_{i2}}{Y_{i1}\tan(\frac{f}{f_1}\theta_{i2}) + Y_{i2}\tan(\frac{f}{f_1}\theta_{i1})} - Y_{i-1}\cot(\frac{f}{f_1}\theta_{i-1}) - Y_i\cot(\frac{f}{f_1}\theta_i), \quad \text{for} \quad i = 1,\cdots,n \tag{5}$$

$$\begin{aligned} b_i(f_r) &= \frac{f_r}{2}\cdot\left.\frac{\partial B_i}{\partial f}\right|_{f=f_r} \\ &= \frac{f_r}{2f_1}\cdot\left\{\frac{Y_{i1}^2\theta_{i2}\sec^2(\frac{f_r}{f_1}\theta_{i2})\tan(\frac{f_r}{f_1}\theta_{i1})}{Y_{i2}\tan(\frac{f_r}{f_1}\theta_{i1}) + Y_{i1}\tan(\frac{f_r}{f_1}\theta_{i2})} + \frac{Y_{i1}^2\theta_{i1}\tan(\frac{f_r}{f_1}\theta_{i2})\sec^2(\frac{f_r}{f_1}\theta_{i1})}{Y_{i2}\tan(\frac{f_r}{f_1}\theta_{i1}) + Y_{i1}\tan(\frac{f_r}{f_1}\theta_{i2})}\right. \\ &\quad + \frac{Y_{i1}\left[Y_{i2} - Y_{i1}\tan(\frac{f_r}{f_1}\theta_{i2})\tan(\frac{f_r}{f_1}\theta_{i1})\right]}{\left[Y_{i2}\tan(\frac{f_r}{f_1}\theta_{i1}) + Y_{i1}\tan(\frac{f_r}{f_1}\theta_{i2})\right]^2}\cdot\left[Y_{i2}\theta_{i1}\sec^2(\frac{f_r}{f_1}\theta_{i1}) + Y_{i1}\theta_{i2}\sec^2(\frac{f_r}{f_1}\theta_{i2})\right] \\ &\quad \left. + Y_{i-1}\theta_{i-1}\csc^2(\frac{f_r}{f_1}\theta_{i-1}) + Y_i\theta_i\csc^2(\frac{f_r}{f_1}\theta_i)\right\}, \quad \text{for } i = 1,\cdots,n \text{ and } r = 1 \text{ or } 2 \end{aligned} \tag{6}$$

where $Y_0 = Y_n = 0$.
Consequently, we can obtain the following equations

$$J_{i,i+1} = \Delta_1 \sqrt{\frac{b_1^2}{g_i g_{i+1}}} = \Delta_2 \sqrt{\frac{b_2^2}{g_i g_{i+1}}}, \quad \text{for} \quad i = 1, \cdots, n-1 \tag{7}$$

$$\Delta_1 b_1 = \Delta_2 b_2 \tag{8}$$

where g_i's are the element values of the prototypical lowpass filter.
The procedures of developing the bandpass filter with controllable dual passbands are provided below.

3.1 Formula development

A. Equal bandwidth ($\Delta_1 f_1 = \Delta_2 f_2$)

With $\theta_{i1} = \theta_{i2} = \theta_i = \theta_0$ and R_f as the ratio of f_2 to f_1, the following equations are derived

$$b_2 = R_f b_1 \tag{9}$$

$$\sec(\theta_0) = -\sec(R_f \theta_0) \tag{10}$$

$$Y_i = \frac{g_0 g_1}{R_S \sqrt{g_i g_{i+1}}} \cdot \sin\theta_0 \tag{11}$$

$$Y_{11} = \frac{g_0 g_1}{R_S \Delta_1 \theta_0} - Y_{1t} \tag{12}$$

$$Y_{i2} = Y_{i1} \cdot \left[\tan^2\theta_0 - \frac{R_S \Delta_1 \theta_0 Y_{it} \sec^2\theta_0}{g_0 g_1} \right] \tag{13}$$

$$Y_{it} = Y_{i-1} + Y_i \tag{14}$$

As the fractional bandwidth of the passband is characterized by the 3 dB band-edge frequency of lower and upper bands, a steeper slope and a narrower bandwidth in the passband may be obtained with an increasing order of the filter. As a result, the formula of Δ_1 needs to be modified. With the assistance of statistical inferences, the orders, Δ_1 and R_f of the proposed dual-passband filter should be in the range of 3-8, 1-21% and 1.5-4, respectively. Therefore the modified formula can be expressed as

$$\Delta_{1m} = MF_{a1} + MF_{a2} \tag{15}$$

where

$$MF_{a1} = 0.9 + (R_f - 1.5)\left[0.5 + 0.2(N-3)\right] + \sum_{i=4}^{N}\left[0.25 + 0.08(i-4)\right] \tag{16}$$

$$MF_{a2} = \begin{cases} (\Delta_1 - 1)\left[MF + 0.01(N-1)\right], & 1\% \le \Delta_1 \le 14\% \\ (\Delta_1 - 1)MF + 0.08(N-1), & 15\% \le \Delta_1 \le 20\% \\ (\Delta_1 - 1)MF, & \Delta_1 = 21\% \end{cases} \tag{17}$$

$$MF = \begin{cases} 0.76, & N = 3 \text{ and } R_f = 1.5 \\ 0.76\left[1.29 + A(N-4)\right], & N \ge 4 \text{ and } R_f = 1.5 \\ 0.76\left[1.29 + A(N-4)\right]\left[1.31 + 0.75(R_f - 2)\right], & N \ge 4 \text{ and } R_f > 1.5 \end{cases} \tag{18}$$

$$A = \begin{cases} 0.18, & 3 \le N \le 5 \\ 0.12, & 6 \le N \le 8 \end{cases} \tag{19}$$

B. Unequal bandwidth ($\Delta_1 f_1 \neq \Delta_2 f_2$)

When the bandwidths of two passbands are unequal, the electrical lengths, θ_{i1} and θ_{i2}, are not equal, either. With $\theta_{i1} = \theta_b$ and $\theta_{i2} = \theta_{i-1} = \theta_i = \theta_a$, the following equations are obtained

$$\left(\frac{B}{C}\right)\Delta_1 = \left(\frac{D}{E}\right)R_f\Delta_2 \tag{20}$$

$$Y_i = \frac{g_0 g_1}{R_S\sqrt{g_i g_{i+1}}} \cdot \sin\theta_a \tag{21}$$

$$Y_{i1} = \frac{-Q + \sqrt{Q^2 - 4PS}}{2P} \tag{22}$$

$$Y_{i2} = \frac{G - H}{K} \tag{23}$$

where

$$\begin{aligned} B = {} & \left[\theta_a \tan\theta_b \sec^2\theta_a + \theta_b \tan\theta_a \sec^2\theta_b\right] \cdot \left[\cot\theta_a \tan\theta_b - \cot(R_f\theta_a)\tan(R_f\theta_b)\right] \\ & + \theta_a \tan\theta_b \csc^2\theta_a \cdot \left[\tan\theta_a \tan\theta_b - \tan(R_f\theta_a)\cdot\tan(R_f\theta_b)\right] + \theta_b \cot\theta_a \sec^2\theta_b \\ & \cdot \left[\tan\theta_a \tan\theta_b + \tan(R_f\theta_a)\tan(R_f\theta_b)\right] \end{aligned} \tag{24}$$

$$C = \tan\theta_a \sec^2\theta_b - \tan(R_f\theta_a)\tan(R_f\theta_b)\cdot\left[\tan\theta_b + \cot\theta_b\right] \tag{25}$$

$$\begin{aligned} D = {} & \theta_a \tan(R_f\theta_b)\sec^2(R_f\theta_a)\cdot\left[\cot\theta_a \tan\theta_b - \cot(R_f\theta_a)\tan(R_f\theta_b)\right] \\ & + \theta_a \tan(R_f\theta_b)\csc^2(R_f\theta_a)\cdot\left[\tan\theta_a \tan\theta_b - \tan(R_f\theta_a)\tan(R_f\theta_b)\right] \\ & + \theta_b \tan\theta_b \sec^2(R_f\theta_b)\cdot\left[\cot\theta_a \tan(R_f\theta_a) - \tan\theta_a \cot(R_f\theta_a)\right] \end{aligned} \tag{26}$$

$$\begin{aligned} E = {} & \tan(R_f\theta_a) - \tan(R_f\theta_a)\tan^2(R_f\theta_b) + \tan\theta_a \tan\theta_b \tan(R_f\theta_b) \\ & - \cot\theta_a \cot\theta_b \tan^2(R_f\theta_a)\tan(R_f\theta_b) \end{aligned} \tag{27}$$

$$G = Y_{i1}^2(\theta_a \tan\theta_b \sec^2\theta_a + \theta_b \tan\theta_a \sec^2\theta_b) \tag{28}$$

$$H = 2Y_{i1}b_1 \tan\theta_a \tag{29}$$

$$K = 2b_1 \tan\theta_b + Y_{it}\theta_b \cot\theta_a \sec^2\theta_b - Y_{it}\theta_a \tan\theta_b \csc^2\theta_a \tag{30}$$

$$P = \theta_a^2 \tan\theta_b \cot\theta_a \sec^4\theta_a + \theta_b^2 \tan\theta_a \cot\theta_b \sec^4\theta_b + 2\theta_a\theta_b \sec^2\theta_a \sec^2\theta_b \tag{31}$$

$$\begin{aligned} Q = {} & 2\left[Y_{it}\theta_a^2 \tan^2\theta_b \sec^2\theta_a \csc^2\theta_a - b_1\theta_a \sec^2\theta_a \sec^2\theta_b + Y_{it}\theta_a\theta_b \tan\theta_a \tan\theta_b \csc^2\theta_a \sec^2\theta_b\right. \\ & \left. - b_1\theta_b \tan\theta_a \sec^2\theta_b(\tan\theta_b + \cot\theta_b)\right] \end{aligned} \tag{32}$$

$$S = Y_{it}^2 \cot\theta_a(\theta_b^2 \cot\theta_b \sec^4\theta_b - \theta_a^2 \tan\theta_b \sec^2\theta_a \csc^2\theta_a) \tag{33}$$

Similarly, the orders, Δ_1 and R_f of the proposed dual-passband filter should be in the range of 3-6, 2-15% and 2.17-3.5, respectively. Therefore the formula of Δ_1 needs to be modified as

$$\Delta_{1m} = \left(MF_{a1} + MF_{a2}\right)\cdot\Delta_1 \tag{34}$$

where

$$MF_{a1} = 1.38 - 0.031(\Delta_1 - 4) + 0.29(N - 3) \tag{35}$$

$$MF_{a2} = 2(R_f - 2.17)\left[0.58 - 0.033(\Delta_1 - 4)\right] \tag{36}$$

3.2 Simulation and Experimental Results

Following are design examples of the three-ordered dual-passband bandpass filters with multilayered structure. Below are fabricated examples categorized by two passbands with equal or unequal bandwidths.

A. Two passbands with equal bandwidth ($\Delta_1 f_1 = \Delta_2 f_2$)

Figure 4 shows the three-ordered dual-passband filter. The central frequencies of two passbands are set at 2 and 5.3 GHz. The bandwidth of both passbands is chosen as 260 MHz, which is 13% of the first passband's central frequency. Moreover, the selected ripple for the prototypical Chebyshev lowpass filter is 0.01 dB. As a result, the electrical length θ_0 and the impedances Z_{11}, Z_{12}, Z_{21}, Z_{22} and Z_1 are obtained as 49.3°, 14.59, 14.64, 17.75, 27.71 and 81.9 Ω, respectively. According to these calculated parameters, theoretical predictions of the dual-passband bandpass filter are shown in Fig. 5*c*. Furthermore, with the assistance of full-wave electromagnetic simulator—Sonnet (Sonnet Software Inc.), these calculated parameters are converted into the multilayered structure.

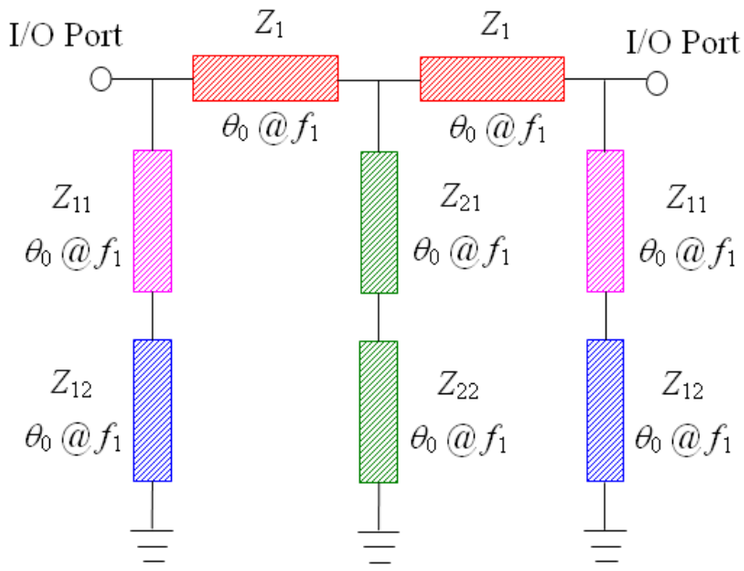

Fig. 4. Architecture of the three-ordered dual-passband filter whose passbands have equal bandwidth

The proposed multilayered dual-passband bandpass filter is fabricated on Dupont 951, whose dielectric constant and loss tangent are 7.8 and 0.0045, respectively. The multilayered 2/5.3 GHz bandpass filter is designed on 11 substrates of 0.09 mm, and its overall size is 4.98 mm × 4.01 mm × 0.99 mm. Figures 5*a* and 5*b* show the 3D architecture and the photograph of this fabricated filter; Fig. 5*c* also presents the measured results.

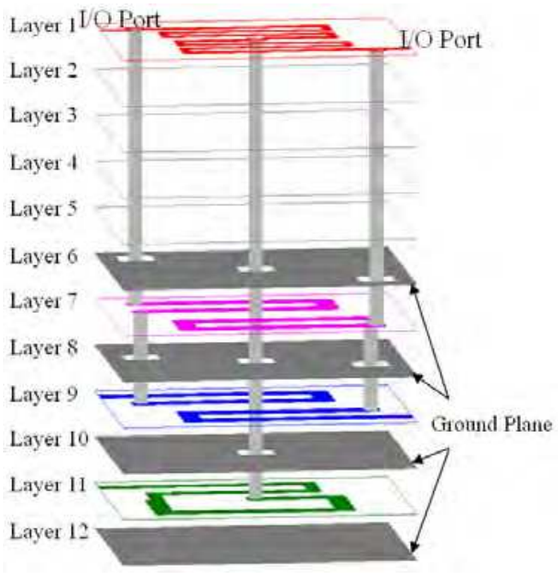

(a) 3D architecture

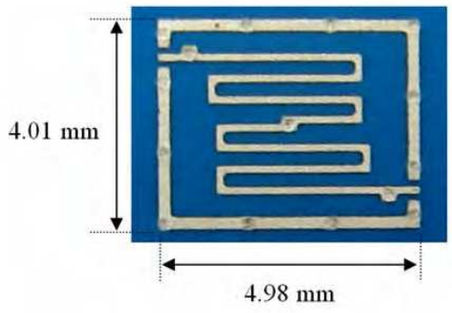

(b) Photograph

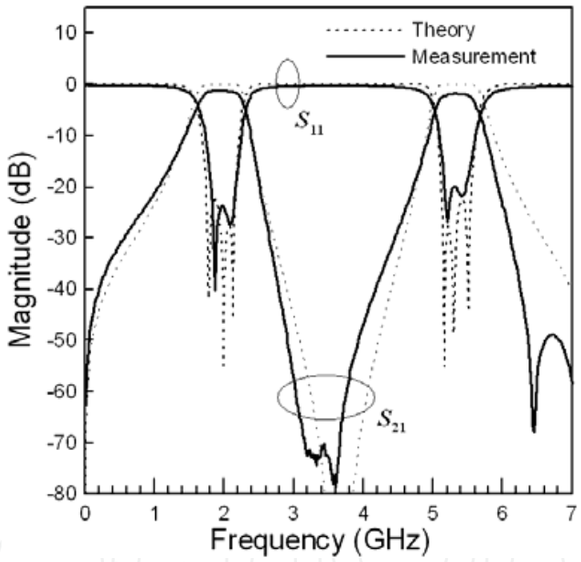

(c) Responses of the theoretical prediction and measurement

Fig. 5. Three-ordered 2/5.3 GHz dual-passband bandpass filter whose passbands have equal bandwidth

On the one hand, within the first passband (1.8-2.2 GHz), the measured insertion loss is < 1.6 dB, whereas the return loss is > 18 dB. On the other hand, within the second passband (5.16-5.51 GHz), the measured insertion loss is < 2.2 dB, whereas the return loss is also > 18 dB.

B. First passband with greater bandwidth ($\Delta_1 f_1 > \Delta_2 f_2$)

Figure 6 shows the architecture of the three-ordered dual-passband filter. The central frequencies of two passbands are set at 2 and 5.3 GHz. The bandwidths of the first and second passband are chosen as 300 and 200 MHz, respectively, which are 15% and 10% of the first passband's central frequency. Moreover, the selected ripple for the prototypical

Chebyshev lowpass filter is 0.01 dB. With the electrical length θ_a as 35.9°, the electrical length θ_b and the impedances Z_{11}, Z_{12}, Z_{21}, Z_{22} and Z_1 are then obtained as 64.3°, 14.17, 13.44, 18.64, 28.34 and 88.24 Ω, respectively. According to these calculated parameters, theoretical predictions of the dual-passband bandpass filter are shown in Fig. 7*c*.

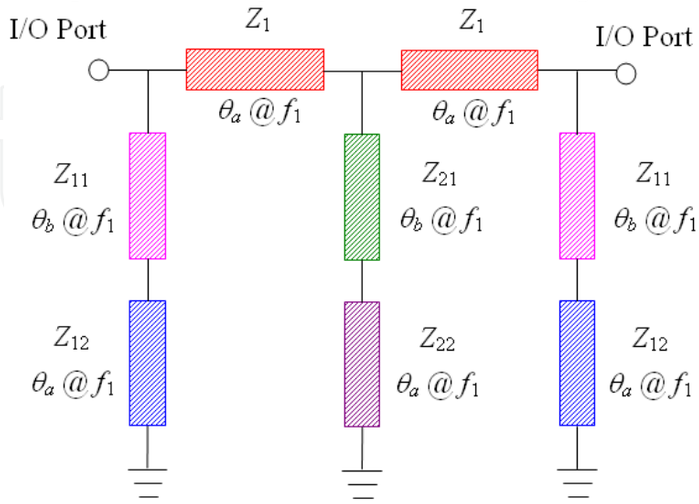

Fig. 6. Architecture of the three-ordered dual-passband filter whose passbands have unequal bandwidths

The multilayered 2/5.3 GHz bandpass filter is fabricated on 12 substrates of 0.09 mm, and its overall size is 4.98 mm × 4.06 mm × 1.08 mm. Figures 7*a* and 7*b* show the 3D architecture and the photograph of this fabricated filter; Fig. 7*c* also presents the measured results.

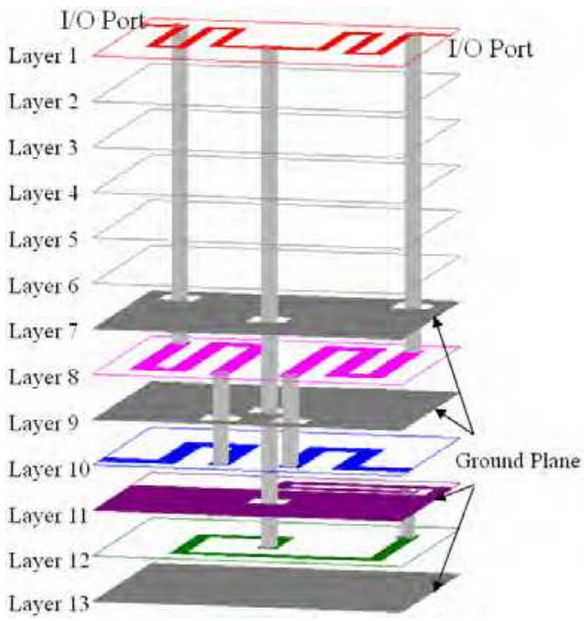

(a) 3D architecture

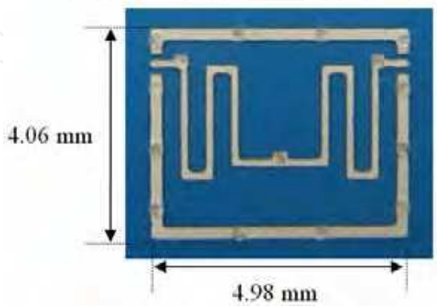

(b) Photograph

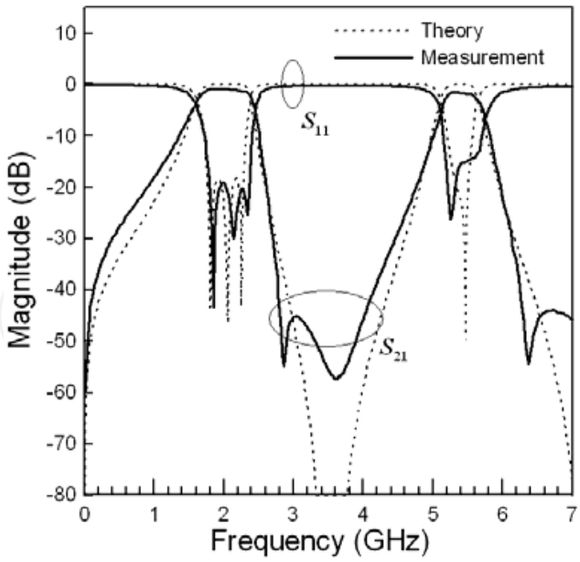

(c) Responses of the theoretical prediction and measurement

Fig. 7. Three-ordered 2/5.3 GHz dual-passband bandpass filter whose first passband's bandwidth is greater

On the one hand, within the first passband (1.79-2.35 GHz), the measured insertion loss is < 1.6 dB, whereas the return loss is > 20 dB. On the other hand, within the second passband (5.2-5.5 GHz), the measured insertion loss is < 2.1 dB, whereas the return loss is > 15 dB.

C. First passband with smaller bandwidth ($\Delta_1 f_1 < \Delta_2 f_2$)

Figure 6 also shows the architecture of the three-ordered dual-passband filter. The central frequencies of two passbands remain as 2 and 5.3 GHz. The bandwidths of the first and second passband are chosen as 200 and 300 MHz, respectively, which are 10% and 15% of first passband's central frequency. Moreover, the selected ripple for the prototypical Chebyshev lowpass filter is 0.01 dB. With the electrical length θ_a as 51°, the electrical length

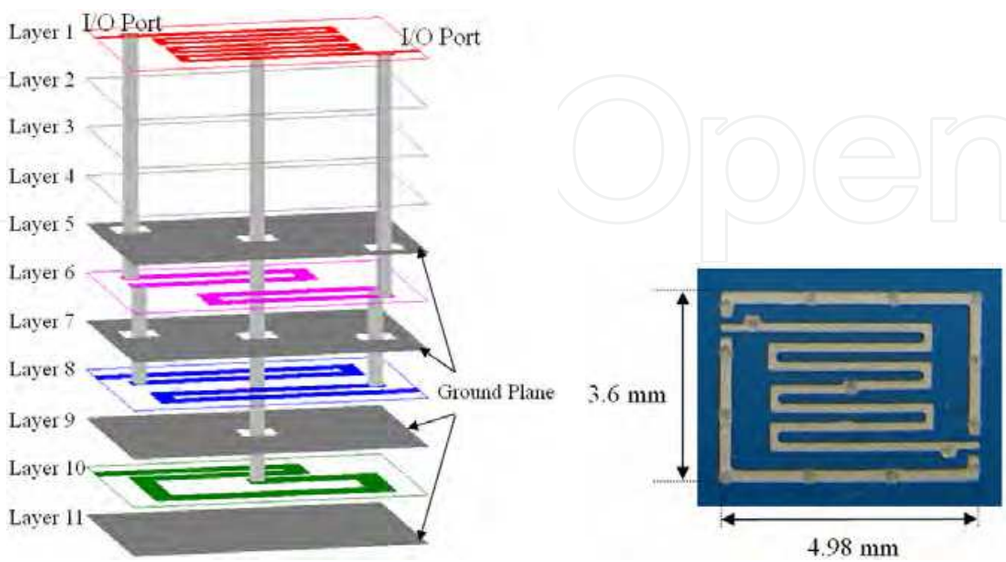

(a) 3D architecture (b) Photograph

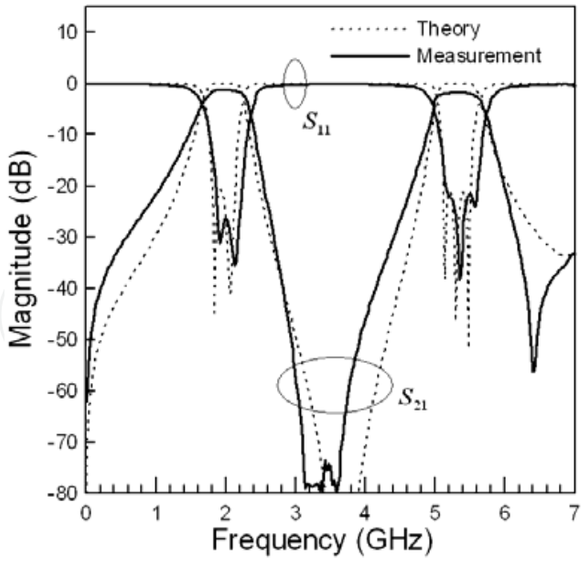

(c) Responses of the theoretical prediction and measurement

Fig. 8. Three-ordered 2/5.3 GHz dual-passband bandpass filter whose first passband's bandwidth is smaller

θ_b and the impedances Z_{11}, Z_{12}, Z_{21}, Z_{22} and Z_1 are then obtained as 47.1°, 11.89, 11.2, 11.28, 13.69 and 74.59 Ω, respectively. According to these calculated parameters, theoretical predictions of the dual-passband bandpass filter are shown in Fig. 8*c*.

The multilayered 2/5.3 GHz bandpass filter is fabricated on 10 substrates of 0.09 mm, and its overall size is 4.98 mm × 3.6 mm × 0.9 mm. Figures 8*a* and 8*b* show the 3D architecture and the photograph of this fabricated filter; Fig. 8*c* also presents the measured results.

On the one hand, within the first passband (1.85-2.22 GHz), the measured insertion loss is < 1.8 dB, whereas the return loss is > 20 dB. On the other hand, within the second passband (5.14-5.62 GHz), the measured insertion loss is < 2.5 dB, whereas the return loss is > 18 dB.

4. Multi-passband filter fabrication

The multi-passband filter can be obtained from (1) to (4). The fabricated examples of triple- and quadruple-passband filters are introduced below.

4.1 Triple-passband filter

Figure 9 shows the architecture of the three-ordered triple-passband filter. The central frequencies of three passbands are set as 2, 5 and 8 GHz. The bandwidths of the first, second and third passband are chosen as 200, 300 and 200 MHz, respectively, which are 10%, 15% and 10% of the first passband's central frequency. Moreover, the selected ripple for the prototypical Chebyshev lowpass filter is 0.01 dB. With the electrical length θ_a as 35.5°, the electrical length θ_b and the impedances Z_{11}, Z_{12}, Z_{13}, Z_{21}, Z_{22}, Z_{23} and Z_1 are then obtained as 37.2°, 20.3, 17.51, 20.34, 29.89, 13.21, 29.84 and 67.7 Ω, respectively. According to these calculated parameters, theoretical predictions of the triple-passband bandpass filter are shown in Fig. 10*c*.

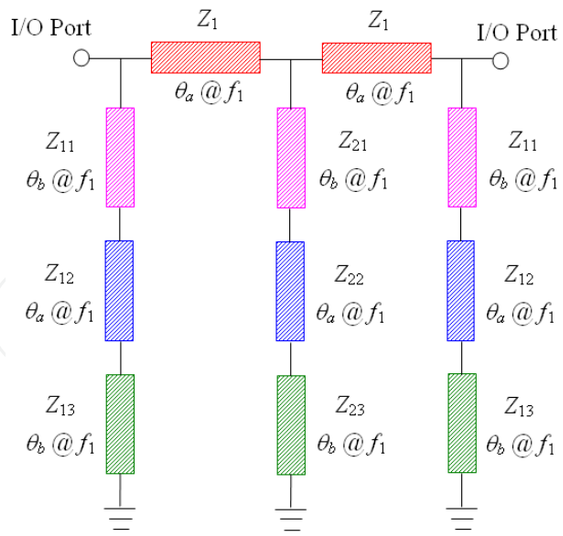

Fig. 9. Architecture of the three-ordered triple-passband filter whose passbands have unequal bandwidths

The multilayered 2/5/8 GHz bandpass filter is fabricated on 10 substrates of 0.09 mm, and its overall size is 4.72 mm × 3.7 mm × 0.9 mm. Figures 10*a* and 10*b* show the 3D architecture and the photograph of this fabricated filter; Fig. 10*c* also presents the measured results.

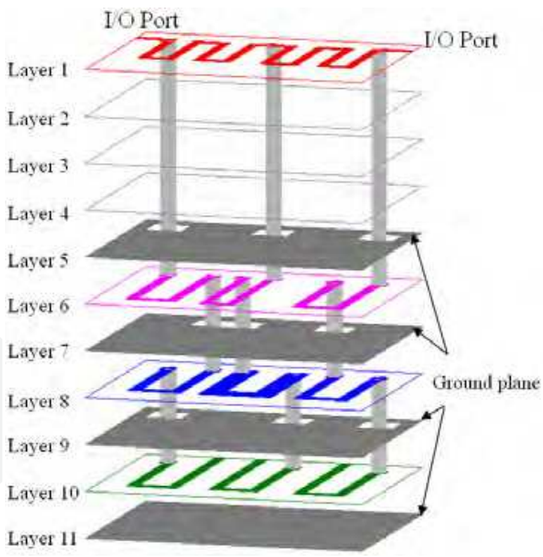

(a) 3D architecture

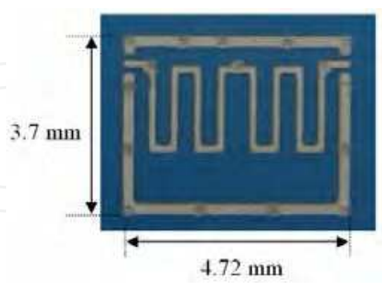

(b) Photograph

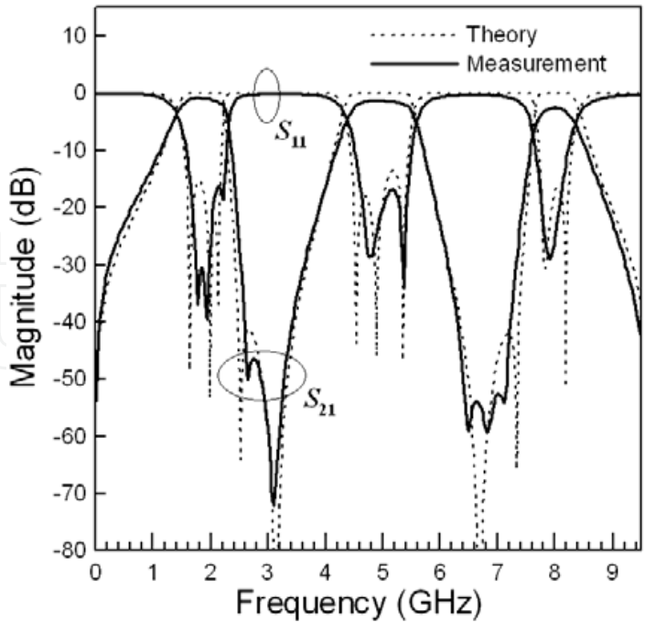

(c) Responses of the theoretical prediction and measurement

Fig. 10. Three-ordered 2/5/8 GHz triple-passband bandpass filter whose second passband's bandwidth is greater

Within the first passband (1.66-2.11 GHz), the measured insertion loss is < 1.4 dB, whereas the return loss is > 16.8 dB. Moreover, within the second passband (4.6-5.35 GHz), the measured insertion loss is < 1.8 dB, whereas the return loss is > 16 dB. Furthermore, within the third passband (7.84-8.14 GHz), the measured insertion loss is < 3 dB, whereas the return loss is > 15 dB.

4.2 Quadruple-passband filter

Figure 11 shows the architecture of the three-ordered quadruple-passband filter. The central frequencies of four passbands are set as 2, 5, 8 and 11.3 GHz. The bandwidth of four passbands is all chosen as 180 MHz, which is 9% of the first passband's central frequency. Moreover, the selected ripple for the prototypical Chebyshev lowpass filter is 0.01 dB. As a result, the electrical length θ_0 and the impedances Z_{11}, Z_{12}, Z_{13}, Z_{14}, Z_{21}, Z_{22}, Z_{23}, Z_{24} and Z_1 are obtained as 26.8°, 21.79, 19.61, 22.74, 14.54, 27.49, 16.01, 14.04, 19.84 and 71.5 Ω, respectively. According to these calculated parameters, theoretical predictions of the quadruple-passband bandpass filter are shown in Fig. 12*c*.

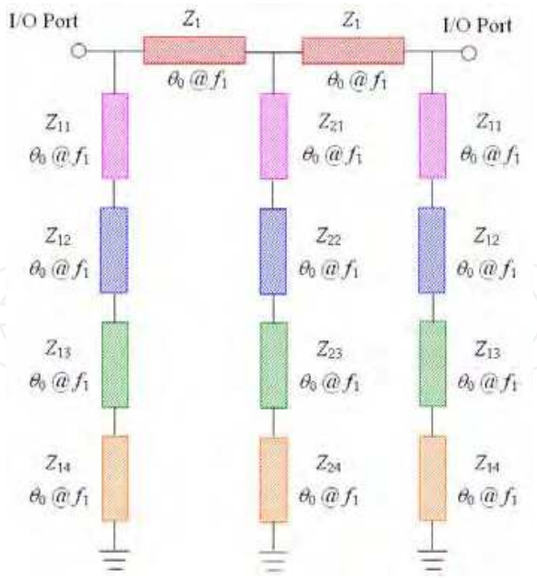

Fig. 11. Architecture of the three-ordered quadruple-passband filter whose passbands have equal bandwidth

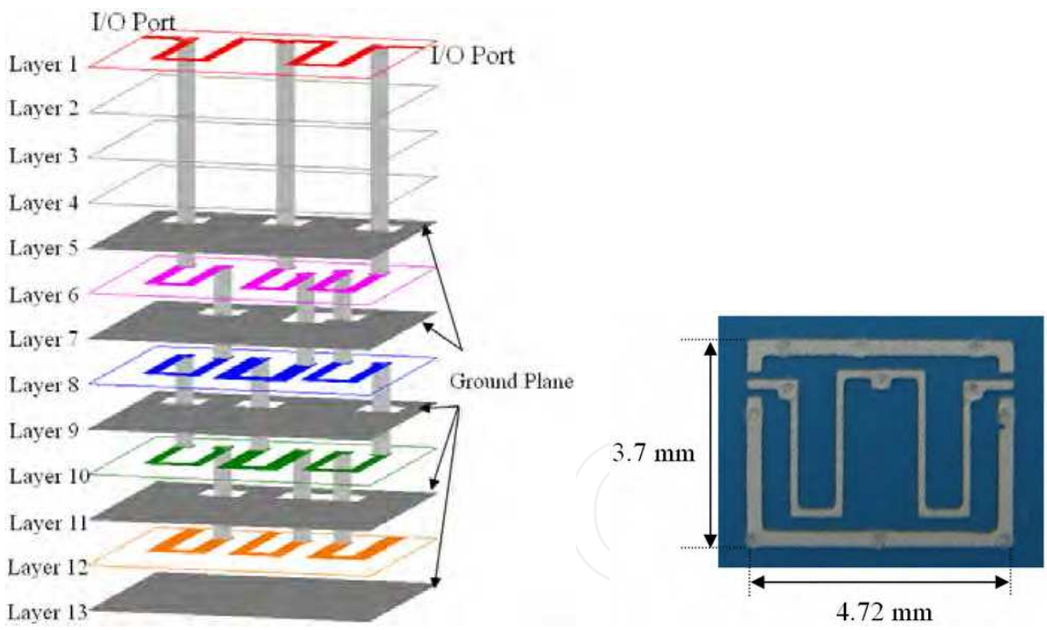

(a) 3D architecture (b) Photograph

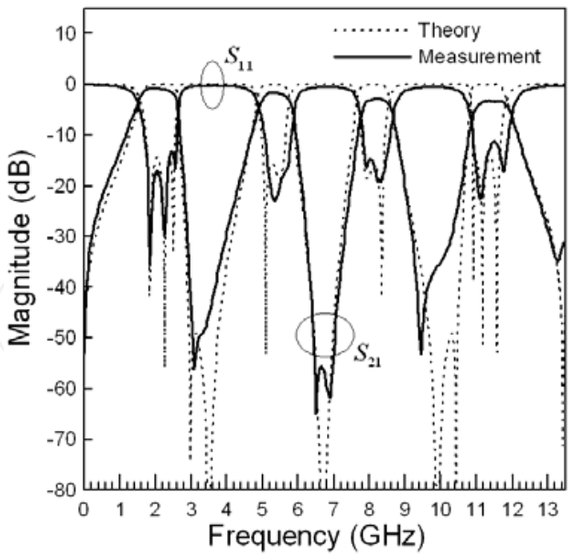

(c) Responses of the theoretical prediction and measurement

Fig. 12. Three-ordered 2/5/8/11.3 GHz quadruple-passband bandpass filter

The multilayered 2/5/8/11.3 GHz bandpass filter is fabricated on 12 substrates of 0.09 mm, and its overall size is 4.72 mm × 3.7 mm × 1.08 mm. Figures 12*a* and 12*b* show the 3D architecture and the photograph of this fabricated filter; Fig. 12*c* also presents the measured results.

Within the first passband (1.77-2.3 GHz), the measured insertion loss is < 1 dB, whereas the return loss is > 17 dB. Moreover, within the second passband (5.14-5.48 GHz), the measured insertion loss is < 1.8 dB, whereas the return loss is > 16 dB. In addition, within the third passband (8.06-8.4 GHz), the measured insertion loss is < 3 dB, whereas the return loss is > 15 dB. Furthermore, within the fourth passband (11.05-11.85 GHz), the measured insertion loss is < 4 dB, whereas the return loss is > 12.5 dB.

5. Conclusion

A novel structure of the multi-passband bandpass filters has been proposed in this article. Multi-sectional short-circuit transmission lines shunted with transmission lines are utilized. By properly choosing the proposed structure's electrical lengths and impedances, multiple passbands can be easily controlled.

In addition, the design procedures have been described in detail, and 3D architectures are provided. Because of the parasitic effect among capacitors for a physical 3D circuit, there is some slight difference between the theoretical predictions and measured results. However, generally speaking, the measured results match well with the theoretical predictions. Therefore with high integration and compact size, the proposed multi-passband filter is suitable for implementation in a multi-chip module.

By the way, because insertion loss measurement is related to the degree and bandwidth of a filter, the performance of a filter with resonators can be well indicated by translating the measurement into an unloaded Q of a resonator.

6. References

[1] Bell, H. C. (2001). Zolotarev bandpass filters, *IEEE Trans. Microw. Theory Tech.*, Vol. 49, No. 12, pp. 2357-2362

[2] Miyake, H.; Kitazawa, S.; Ishizaki, T.; Yamada, T. & Nagatomi, Y. (1997). A miniaturized monolithic dual band filter using ceramic lamination technique for dual mode portable telephones, *Proceedings of IEEE MTT-S Int. Microw. Symp. Dig.*, pp. 789-792

[3] Quendo, C., Rius, E. & Person, C. (2003). An original topology of dual-band filter with transmission zeros, *Proceedings of IEEE MTT-S Int. Microw. Symp. Dig.*, pp. 1093-1096

[4] Chang, C. H.; Wu, H. S.; Yang, H. J. & Tzuang, C. K. C. (2003). Coalesced single-input single-output dual-band filter, *Proceedings of IEEE MTT-S Int. Microw. Symp. Dig.*, pp. 511-514

[5] Tsai, C. M.; Lee, H. M. & Tsai, C. C. (2005). Planar filter design with fully controllable second passband, *IEEE Trans. Microw. Theory Tech.*, Vol. 53, No. 11, pp. 3429-3439

[6] Yim, H. Y. & Cheng, K. K. M. (2005). Novel dual-band planar resonator and admittance inverter for filter design and applications, *Proceedings of IEEE MTT-S Int. Microw. Symp. Dig.*, pp. 2187-2190

[7] Lee, J.; Uhm, M. S. & Yom, I. B. (2004). A dual-passband filter of canonical structure for satellite applications, *IEEE Microw. Wireless Comp. Lett.*, Vol. 14, No. 6, pp. 271-273

[8] Kuo, J. T.; Yeh, T. H. & Yeh, C. C. (2005). Design of microstrip bandpass filters with a dual-passband response, *IEEE Trans. Microw. Theory Tech.*, Vol. 53, No. 4, pp. 1331-1337

[9] Chen, C. C. (2005). Dual-band bandpass filter using coupled resonator pairs, *IEEE Microw. Wireless Comp. Lett.*, Vol. 15, No. 4, pp. 259-261

[10] Rong, Y.; Zaki, K. A.; Hageman, M.; Stevens, D. & Gipprich, J. (1999). Low temperature cofired ceramic (LTCC) ridge waveguide bandpass filters. *Proceedings of IEEE MTT-S Int. Microw. Symp. Dig.*, pp. 1147-1150

[11] Heo, D.; Sutono, A.; Chen, E.; Suh, Y. & Laskar, J. (2001). A 1.9 GHz DECT CMOS power amplifier with fully integrated multilayer LTCC passives, *IEEE Microw. Wireless Comp. Lett.*, Vol. 11, No. 6, pp. 249-251

[12] Leung, W. Y.; Cheng, K. K. M. & Wu, K. L. (2001). Design and implementation of LTCC filters with enhanced stop-band characteristics for bluetooth applications. *Proceedings of Asia-Pacific Microw. Conf.*, pp. 1008-1011

[13] Tang, C. W.; Sheen, J. W. & Chang, C. Y. (2001). Chip-type LTCC-MLC baluns using the stepped impedance method, *IEEE Trans. Microw. Theory Tech.*, Vol. 49, No. 12, pp. 2342-2349

[14] Tang, C. W.; Lin, Y. C. & Chang, C. Y. (2003). Realization of transmission zeros in combline filters using an auxiliary inductively-coupled ground plane, *IEEE Trans. Microw. Theory Tech.*, Vol. 51, No. 10, pp. 2112-2118

[15] Tang, C. W. (2004). Harmonic-suppression LTCC filter with the step impedance quarter-wavelength open stub, *IEEE Trans. Microw. Theory Tech.*, Vol. 52, No. 2, pp. 617-624

[16] Tang, C. W.; You, S. F. & Liu, I. C. (2006). Design of a dual-band bandpass filter with low temperature co-fired ceramic technology, *IEEE Trans. Microw. Theory Tech.*, Vol. 54, No. 8, pp. 3327-3332

[17] Sun, S. & Zhu, L. (2006). Novel design of microstrip bandpass filters with a controllable dual-passband response: description and implementation, *IEICE Trans. Electron.*, Vol. E89-C, No. 2, pp.197-202

[18] Quendo, C.; Manchec, A.; Clavet, Y.; Rius, E.; Favennec, J. F. & Person, C. (2007). General Synthesis of N-Band Resonator Based on N-Order Dual Behavior Resonator, *IEEE Microw. Wireless Comp. Lett.*, Vol. 17, No. 5, pp. 337-339

[19] Matthaei, G.L.; Young, L. & Jones, E.M. (1980). *Microwave filters, impedance-matching network, and coupling structures*, Artech House, Norwood, MA

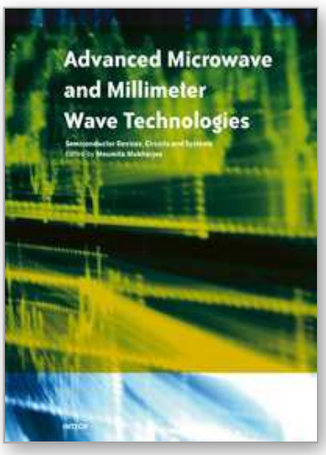

Advanced Microwave and Millimeter Wave Technologies
Semiconductor Devices Circuits and Systems
Edited by Moumita Mukherjee

ISBN 978-953-307-031-5
Hard cover, 642 pages
Publisher InTech
Published online 01, March, 2010
Published in print edition March, 2010

This book is planned to publish with an objective to provide a state-of-the-art reference book in the areas of advanced microwave, MM-Wave and THz devices, antennas and systemtechnologies for microwave communication engineers, Scientists and post-graduate students of electrical and electronics engineering, applied physicists. This reference book is a collection of 30 Chapters characterized in 3 parts: Advanced Microwave and MM-wave devices, integrated microwave and MM-wave circuits and Antennas and advanced microwave computer techniques, focusing on simulation, theories and applications. This book provides a comprehensive overview of the components and devices used in microwave and MM-Wave circuits, including microwave transmission lines, resonators, filters, ferrite devices, solid state devices, transistor oscillators and amplifiers, directional couplers, microstripeline components, microwave detectors, mixers, converters and harmonic generators, and microwave solid-state switches, phase shifters and attenuators. Several applications area also discusses here, like consumer, industrial, biomedical, and chemical applications of microwave technology. It also covers microwave instrumentation and measurement, thermodynamics, and applications in navigation and radio communication.

INTECH
open science | open minds

InTech Europe
University Campus STeP Ri
Slavka Krautzeka 83/A
51000 Rijeka, Croatia
Phone: +385 (51) 770 447
Fax: +385 (51) 686 166

InTech China
Unit 405, Office Block, Hotel Equatorial Shanghai
No.65, Yan An Road (West), Shanghai, 200040, China
中国上海市延安西路65号上海国际贵都大饭店办公楼405单元
Phone: +86-21-62489820
Fax: +86-21-62489821

IntechOpen

IntechOpen